Realization of exciton-polariton condensation in GaAs-based microcavity grown by metalorganic chemical vapor deposition

Daegwang Choi, Min Park, Chan-Young Sung, Hyoungsoon Choi, and Yong-Hoon Cho*

Department of Physics and KI for the NanoCentury,
Korea Advanced Institute of Science and Technology (KAIST), Daejeon 34141, Republic of Korea

(Received 28 February 2022; revised 4 August 2022; accepted 9 August 2022; published 6 September 2022)

Metalorganic chemical vapor deposition (MOCVD) has not been often used for studying exciton-polariton condensation and developing polaritonic devices, although it is a powerful mass productive method for practical applications. Here, we demonstrate that the MOCVD-grown GaAs-based microcavity can realize the nonequilibrium condensation of exciton-polariton. We obtained the Rabi splitting values of 10.1 meV in the angle-resolved reflectance spectrum from the MOCVD-grown microcavity. And, we also measured the angle-resolved photoluminescence depending on pumping power to observe condensation behaviors. Furthermore, we found that the occupancy distributions of polaritons are in a nonequilibrium state by fitting Bose-Einstein distributions. To realize the strong coupling and exciton-polariton condensation, we reduced the linewidth broadening of photoluminescence from quantum wells by optimizing growth conditions and designs.

DOI: 10.1103/PhysRevResearch.4.033188

I. INTRODUCTION

Since the first observation of Bose-Einstein condensation in exciton-polariton (polariton) in 2006 [1], which was achieved with CdTe-based microcavities grown by molecular beam epitaxy (MBE), the research of polaritons has flourished for more than a decade. Polariton condensations have revealed numerous interesting phenomena such as superfluidity [2], quantized vortex [3], soliton [4], and simulating artificial lattice [5]. Moreover, versatile applications using polaritons have been studied, such as polariton laser [6,7], light-emitting device [8], logic device [9], topological insulator [10], and quantum computing [11].

Recently, various attempts to practically utilize polariton condensates are currently underway. Several novel materials, such as wide band-gap semiconductor [12], organic material [13], perovskite [14], and transition metal dichalcogenide [15], have recently been investigated to realize polariton condensates at room temperature. Although GaAs-based microcavities require cryostat temperature to form polariton condensates due to their small exciton binding energy [16], the GaAs still have advantages when considering large area fabrication and electrically driven operation. Moreover, a recent report showed that the AlGaAs-based microcavity could also achieve strong coupling even at room temperature [17].

In a GaAs-based planar microcavity, although the coupled exciton-photon mode splitting was observed in a GaAs-based microcavity grown by metalorganic chemical vapor deposition (MOCVD) in 1992 [18], condensation has been reported after that for MBE-grown GaAs microcavities [19,20]. Since then, several groups have attempted to grow microcavities for polaritons using MOCVD [21–24], MOCVD handed over the supremacy to MBE due to relatively higher material quality. Nowadays, MBE has reached the level of growing microcavities with a quality factor (Q factor) of 10^5 order and reaching thermal equilibrium of polaritons [25].

However, MOCVD has its advantages in terms of mass productivity for practical applications [26]. The growth rate of MOCVD is one order of magnitude higher than that of MBE, and MOCVD can grow many and larger wafers at once. For instance, in order to grow the sophisticated polariton-based microcavity samples with top and bottom distributed Bragg reflectors (DBRs) and several sets of multiple quantum wells (MQWs), MBE typically requires more than 1 d while 6 h are enough for MOCVD. Furthermore, industries have already used MOCVD for a vertical-cavity surface-emitting laser (VCSEL) with GaAs-based systems [27]. Even though polariton-based microcavities need further requirements than VCSEL for a strong-coupling regime, the practical use of MOCVD-grown polariton devices could be feasible enough.

To realize polariton condensates, the first requirement is satisfying a strong-coupling regime, and the second requirement is the higher polariton density than critical density in principle. However, it can be expressed that a high-quality structure is needed phenomenologically. Although early results do not directly mention the Q factor of the samples, we can estimate them with data. Early MBE-grown microcavities that showed condensation behavior had an order of 10^3 Q factor [19,20]. However, early MOCVD-grown microcavities are assumed to show an order of 10^2 Q factor [21–23]. These days, MOCVD also can produce a high-quality structure of DBRs with a reflectivity (R) >99.98% [28] or MQWs

*yonghcho@kaist.ac.kr

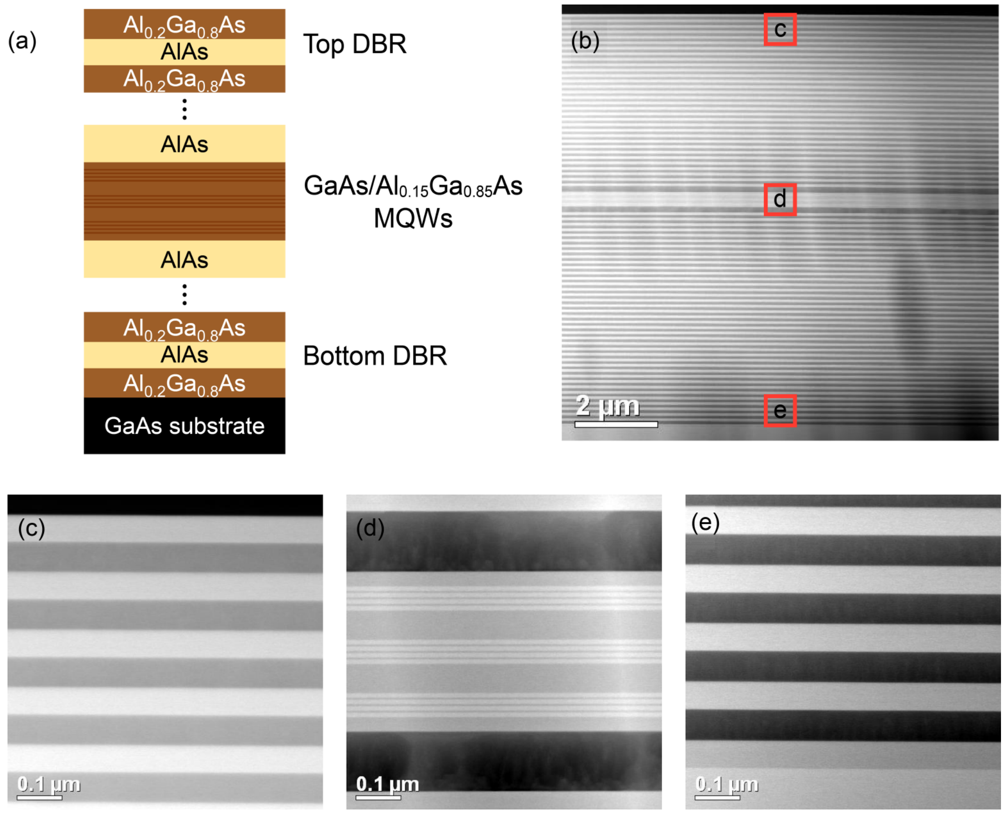

FIG. 1. Sample information. (a) Simple illustration of a GaAs-based planar microcavity structure. Sample forms a $3\lambda/2$ optical cavity between two DBRs consisting of 32.5 and 39.5 pairs of $AlAs/Al_{0.2}Ga_{0.8}As$. The cavity contains three sets of four MQWs consisting of $GaAs/Al_{0.15}Ga_{0.85}As$ in the antinode of an electric field. (b) Cross-sectional TEM images of the whole microcavity structure. Red boxes indicate the position of the images (c)–(e), which show top DBR, cavity region with MQWs, and bottom DBR, respectively.

with a linewidth (ΔE) <1.0 meV [29], respectively. The Rabi splitting value in a GaAs-based microcavity is typically about 4–15 meV [30]. We note that ΔE from MOCVD is already narrower than the typical Rabi splitting value. However, MOCVD has not been paid much attention to for realizing polariton condensation.

In this work, we demonstrate the nonequilibrium polariton condensation in a *MOCVD-grown* AlGaAs-based microcavity. The sample consists of $AlAs/Al_{0.2}Ga_{0.8}As$ top and bottom DBRs and contains $GaAs/Al_{0.15}Ga_{0.85}As$ MQWs. To satisfy the strong-coupling condition, we optimized the growth condition of the MQW structure to minimize the linewidth broadening of the MQW emission. We also measure the transmission electron microscope (TEM) measurement to show the cross section of the structure. Furthermore, we measured the reflectance spectrum to observe the reflectance dip of two polariton branches. To see clear anticrossing behavior, we etched the top DBR structure with a selective wet etching process. We measured the clear Rabi splitting and found that it depends on the number of top DBRs. We measured angle-resolved photoluminescence (PL) spectra according to pumping power. Polaritons form a condensates state above the threshold density as the pumping power increases. And we plotted intensity curves, linewidth, and blueshift according to pumping power. Furthermore, we measured PL spectra using a continuous-wave (cw) laser to obtain the occupancy of polaritons for different pumping powers.

II. EXPERIMENTAL RESULTS

The sample used in the experiments is a GaAs-based planar microcavity grown by MOCVD on a GaAs substrate. The microcavity contains 32.5 and 39.5 pairs of $AlAs/Al_{0.2}Ga_{0.8}As$ DBRs on the top and bottom sides. The sample has three sets of four $GaAs/Al_{0.15}Ga_{0.85}As$ MQWs at the antinodes of the electric fields in the cavity, which are sandwiched by two DBRs to form an $3\lambda/2$ optical cavity. The thickness of the GaAs well was designed to 10 nm, and the $Al_{0.15}Ga_{0.85}As$ barrier was designed to 4 nm. The wavelength of cavity mode and the MQW were designed around 800 nm at 5 K. Figure 1(a) illustrates the sample structure, and Fig. 1(b) shows the cross-sectional TEM image of the whole microcavity structure. Figures 1(c)–1(e) show TEM images of top DBR, MQWs, and bottom DBR, respectively. The red boxes in Fig. 1(b) indicate the position of each magnified TEM image shown in Figs. 1(c)–1(e). We could obtain well-controlled abrupt interfaces between layers.

The optical measurements were conducted at 5 K with an optical cryostat. Firstly, we measured angle-resolved reflectance spectra to obtain the Rabi splitting value and to observe polariton branches. However, the high reflectance of the top DBR caused difficulties in measuring the reflectance dip of polariton branches. Figure 2(a) shows only a weak signal of the lower polariton branch. So, we partially removed top DBRs by a selective wet etching process to confirm the strong coupling of the microcavity. AlAs and $Al_{0.2}Ga_{0.8}As$

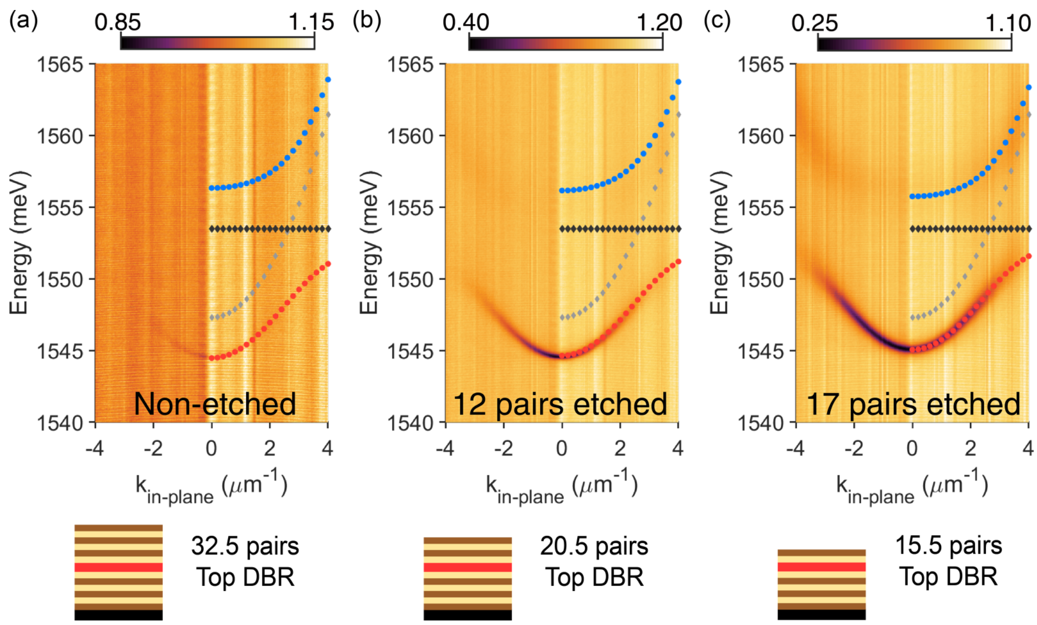

FIG. 2. Reflectance spectra for measuring Rabi splitting values depending on the number of top DBRs. Angle-resolved reflectance spectra of (a) nonetched (i.e., 32.5 pairs) microcavity, (b) 12 pairs of top DBR-etched (i.e., 20.5 pairs) microcavity, (c) 17 pairs of top DBR-etched (i.e., 15.5 pairs) microcavity. Dotted black and gray lines show fitted energies of QW excitons and cavity mode, respectively. The red and blue lines show fitted energies of lower and upper polariton branches. The measured Rabi splitting values are 10.1, 9.7, and 8.7 meV for (a), (b), and (c), respectively. Reflectance dip signals of lower polariton branches in reflectance spectra are blueshifted and broadened by wet etching of top DBRs due to reduced Rabi splitting.

layers of top DBRs can be selectively etched by two kinds of wet etchants [31,32]. We used the mixture of citric acids and hydrogen peroxide solution to etch the $Al_{0.2}Ga_{0.8}As$ layer and used the mixture of phosphoric acid and hydrogen peroxide solution to etch the AlAs layer. The used phosphoric acid mixture has $50:3:1 =$ deionized water:phosphoric acid:hydrogen peroxide. And the citric acid is made by citric acid anhydrous powder with deionized water as a 1:1 mass ratio (e.g., 100 g powder and 100 ml water). The used citric acid mixture has $8:1 =$ citric acid solution:hydrogen peroxide. The temperature of each solution is about 30 °C. We immersed the piece of microcavity into each acid for a few seconds and washed it with the deionized water every time before immersing it in other acid solutions. Thus, we fabricated 12 and 17 pairs of DBR-etched microcavities using the wet etching process. We note that the nonetched and etched samples are from an identical wafer. We diced the wafer into small pieces having 1 mm^2 area for the wet etching process. The etched sample also had similar optical properties to the nonetched one before etching. After the wet etching process, we could observe clear anticrossing behavior and upper polariton branches. Figures 2(b) and 2(c) show the angle-resolved reflectance spectra of 12 pairs of DBR-etched and 17 pairs of DBR-etched (i.e., 20.5 and 15.5 DBR pairs remained) microcavities. We fitted the energy-momentum distribution of lower and upper polariton branches with the red and blue dotted lines in Figs. 2(a)–2(c). The black and gray dotted lines indicate the fitting curves of the energy of the quantum well (QW) exciton and cavity modes. The QW exciton is at 1553.5 meV, and the cavity mode is at 1547.3 meV. So, the detuning between the cavity mode and QW exciton is negative with $\Delta = -6.2$ meV. The measured Rabi splitting values of the nonetched, 12, and 17 pairs of DBR-etched samples are 10.1, 9.7, and 8.7 meV, respectively. With decreasing top DBR, the reflectance dip signals become deeper and more broadened. The reduced top DBR degraded the photonic cavity and decreased Rabi splitting values because the spatial overlap between exciton and cavity modes was reduced. From the detuning and Rabi splitting value, we can obtain the Hopfield coefficients [33] such as $|C|^2 = \frac{1}{2}\frac{\sqrt{\Delta^2+\Omega^2}-\Delta}{\sqrt{\Delta^2+\Omega^2}}$, $|X|^2 = \frac{1}{2}\frac{\sqrt{\Delta^2+\Omega^2}+\Delta}{\sqrt{\Delta^2+\Omega^2}}$. In the nonetched sample, we obtained the fraction of photonic and excitonic parts of the lower polariton branch, $|C|^2 = 0.76$, $|X|^2 = 0.24$.

We also measured the angle-resolved PL spectrum with increasing pumping power. We used a fs-pulsed Ti:sapphire laser with an energy of 1.72 eV (723.0 nm) to excite the sample nonresonantly. The laser has a broad Gaussian shape with a beam diameter of $\sim 35\ \mu$m to exclude localized effects or potential gradients [34,35]. Figure 3(a) shows the PL emissions with broad energy-momentum distribution in lower polariton branches at a low power pumping case. The linewidth of the lower polariton branch at $k = 0\ \mu\text{m}^{-1}$ is about 0.13 meV when $P = 0.02\ P_{\text{th}}$. The experimental Q factor of the cavity can be deduced from the linewidth value of the lower polariton branch [36,37]. The Q factor of the sample we used can be at least about $\sim \frac{1545}{0.13/0.76} \sim 9 \times 10^3$. As the pumping power increases, the polaritons experience blueshift due to polariton-polariton interaction [Fig. 3(b)]. The red dotted line shows the initial energy level as a guideline. Above the threshold density, the polaritons condensed to the ground state at $k = 0\ \mu\text{m}^{-1}$ with more blueshift [Fig. 3(c)]. Furthermore, the PL emission follows the lower polariton branch with linewidth broadening [Figs. 3(d)–3(f)]. We also observed

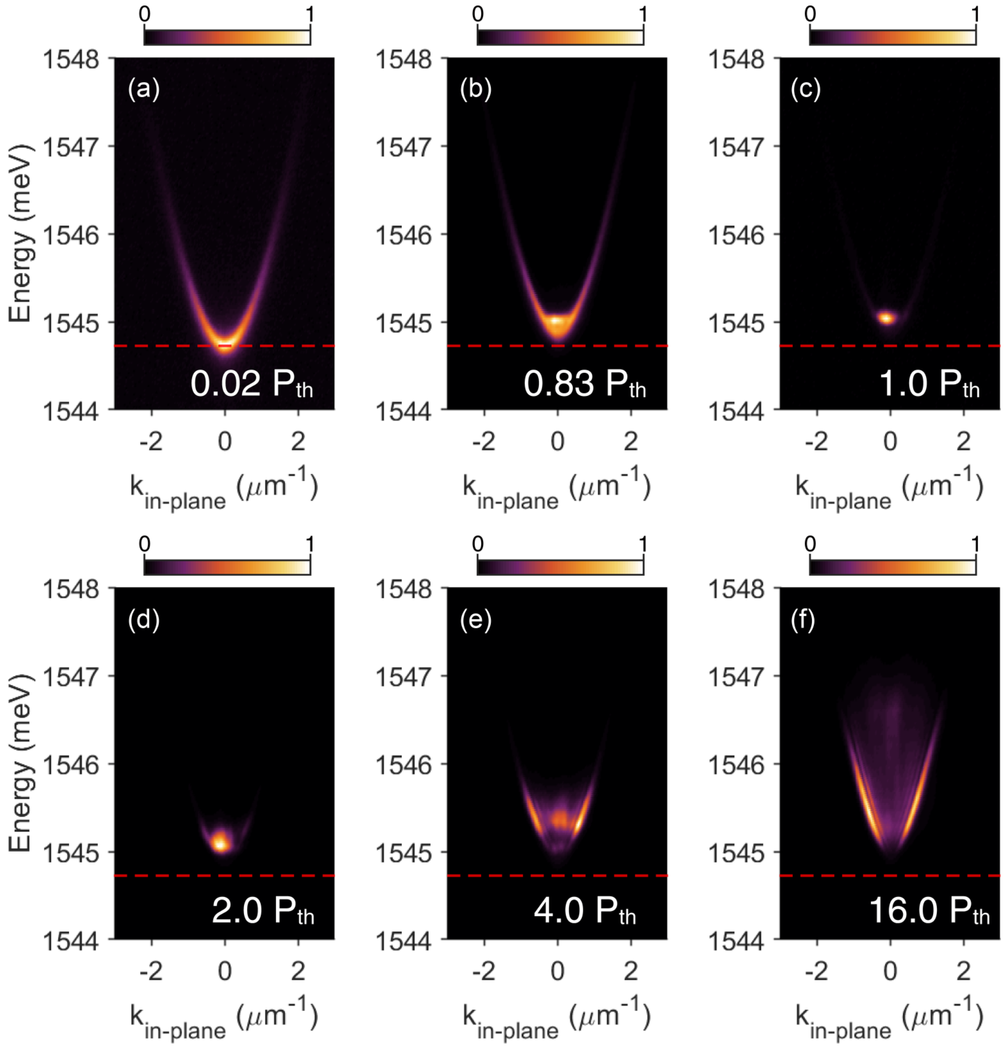

FIG. 3. Angle-resolved PL spectra according to pumping power. From (a) to (f), the pumping power is $0.02P_{\mathrm{th}}$, $0.83P_{\mathrm{th}}$, $1.0P_{\mathrm{th}}$ $2.0P_{\mathrm{th}}$, $4.0P_{\mathrm{th}}$, and $16.0P_{\mathrm{th}}$ respectively. P_{th} is about 0.8 μW/μm^2. Above the threshold density, lower polaritons condensed to a single ground state. As pumping power increases, dispersions become broadened and follow the lower polariton branches.

the condensates having finite k above the $P = 2.0P_{\mathrm{th}}$. These condensates can be understood as the ballistic motion of polaritons by the potential gradient from the blueshifted central spot [38]. These phenomena are much more easily observed in tightly focused beam excitation due to the steep potential gradient from the pumping spot (shown in Fig. S.2 in the Supplemental Material [39]).

We plotted the pumping power dependency in PL intensity (black square), blueshift (red circle), and linewidth (blue diamond) of PL emission in Fig. 4. We extracted the PL spectrum of the ground state at $k = 0$ μm^{-1} from Fig. 3. Below the threshold density, the PL intensity shows just a linear increase, whereas at around the threshold density, the PL intensity shows a nonlinear increase. The threshold pumping power for condensation is about 0.8 μW/μm^2. However, the PL intensity of the ground state is not linearly increased far above the threshold density. Although the total intensity of PL emission is increased (shown in Fig. S.1 in the Supplemental Material), the intensity of PL at $k = 0$ μm^{-1} was almost constant. It is because the portions of PL emission at $k \neq 0$ μm^{-1} are increased above the $P \sim 2P_{\mathrm{th}}$, as shown in Figs. 3(d)–3(f). The PL peak of polariton condensates also showed the linewidth narrowing above the threshold density. The blueshift of the PL peak is also observed with increasing polariton density. The linewidth of PL emission is decreased to about 80 μeV after condensation. As the pumping power increases further, the linewidth increases again due to the increased polariton-polariton interactions.

III. OCCUPANCY OF POLARITONS

Furthermore, we measured the occupancy of lower polaritons from PL spectra using a cw Ti:sapphire laser with an energy of 1.71 eV (725.0 nm) at 5 K. We used an optical chopper to avoid laser heating. The laser also has a Gaussian shape with a beam diameter of 35 μm. And we used a spatial filter with a diameter of 22 μm to collect emissions from a filtered area at the center of the excitation spot. We deduced the occupancy of polaritons from angle-resolved PL spectra for various pumping powers, shown in Fig. 5. The measured PL spectra only show the $k_x = 0$ slices with a spectrometer slit in the vertical direction. So, we extrapolated the polariton

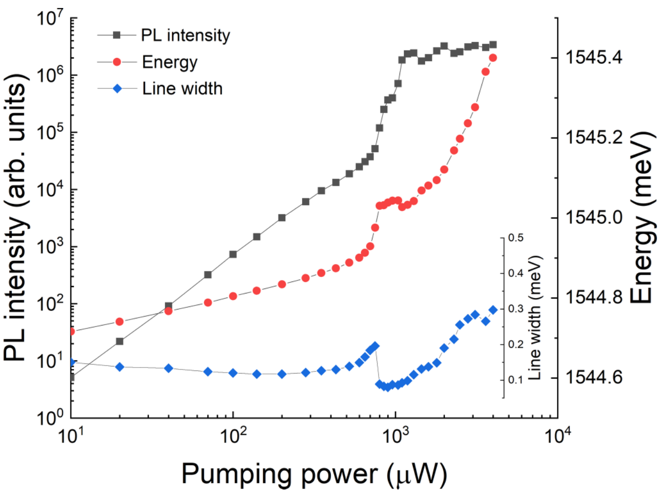

FIG. 4. Pumping power dependence of polariton condensates. PL intensity of ground state at $k = 0\ \mu\mathrm{m}^{-1}$ (black square), the energy of ground state (red circle), and linewidth of PL emission (blue diamond). Integrated PL intensity indicates occupancy of the ground state, which shows nonlinear increases around threshold density. The energy of the ground state is increased due to the repulsive interaction between polaritons. And the linewidth of polariton emissions becomes narrower above the threshold of condensation. After the condensation, the linewidth is again increased due to the increased interactions.

density at $k_x \neq 0$ by assuming rotational invariance in k space. And we considered the detection efficiencies of the optical setup, the grating, and the CCD in the spectrometer. And, we considered the number of the state in a single CCD pixel, which has a finite size in k-space measurement. We follow

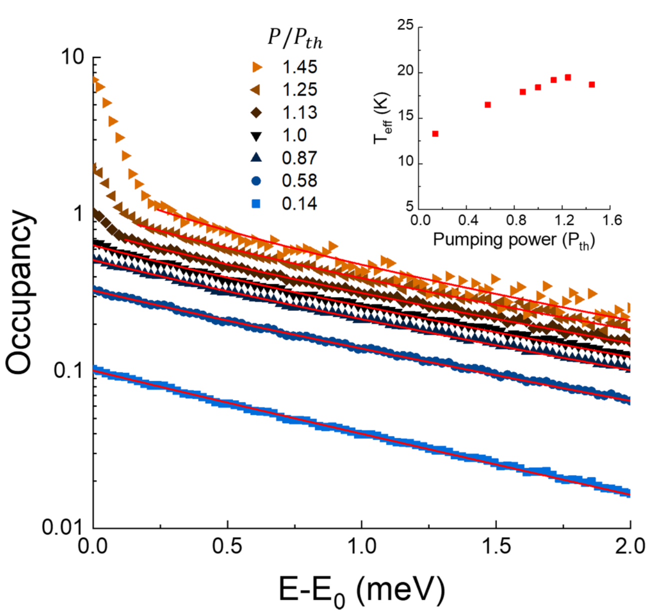

FIG. 5. Occupancy of lower polaritons for various pumping powers. The occupancy is deduced from the angle-resolved PL spectrum data at 5 K using a cw laser. All occupancies are fitted by Bose-Einstein distribution with each effective temperature T_{eff}. Fitting curves are plotted with red lines. Inset shows fitted T_{eff} with different pumping power.

the calculations in the Supplemental Material of Ref. [25], with different parameters given by the collected area of emission with a spatial filter $A_{\mathrm{obs}} = 379.9\ \mu\mathrm{m}^2$, the range of momentum space by one CCD pixel $\Delta k = 0.036\ \mu\mathrm{m}^{-1}$, the efficiency of CCD in the spectrometer $\eta_{\mathrm{CCD}} = 0.5$, the efficiency of the grating in the spectrometer $\eta_{\mathrm{grating}} = 0.8$, the efficiency of the optical setup from the cryostat window to the spectrometer $\eta_{\mathrm{setup}} = 0.48$, and the assumed polariton lifetime $\tau_{\mathrm{pol}} = 5 \times 10^{-12}$ s. The duty cycle of the optical chopper (d) is 0.5. The polariton lifetime is assumed from the cavity quality factor. The setup efficiency is measured by the laser with an 800 nm wavelength (the emission wavelength of the lower polariton). The setup contains mirrors, lenses, a dichroic beam splitter, and a cryostat window. We took the efficiencies of the CCD and grating from the specification data of our equipment at 800 nm. All distributions in Fig. 5 are compared to the Bose-Einstein distribution (plotted with red lines), given by

$$N(E) = \frac{1}{e^{(E-\mu)/k_B T_{\mathrm{eff}}} - 1}, \tag{1}$$

where T_{eff} is effective temperature, μ is chemical potential of polaritons, and k_B is the Boltzmann constant. Below the threshold, distributions showed linear relations in the logarithmic scale, which are close to the Maxwell-Boltzmann distribution. However, above the threshold ($P > 1.0P_{\mathrm{th}}$), the occupancy of the low-energy states increased, and we could not find reasonable fittings for the low-energy states. This can be explained as polaritons are nonideal bosonic systems [1]. Furthermore, the T_{eff} can be well fitted with high-energy tails in all distributions, shown in the inset of Fig. 5. The T_{eff} are higher than the cryostat temperature (= 5 K), and the T_{eff} changes with different polariton densities. Thus, the created polaritons are not fully thermalized and condensates are in a *nonequilibrium* state [20].

IV. SAMPLE GROWTH TO ACHIEVE STRONG COUPLING

To satisfy the strong-coupling condition and realize polariton condensates in a MOCVD-grown microcavity, we have tried to reduce linewidth broadening in the PL emission from our MQW structures. Although MOCVD-grown DBRs exhibit a high-quality cavity mode to achieve strong-coupling conditions, the MQW emissions typically show a broader linewidth than MBE samples even at low temperatures. We have grown the only MQW structure without a DBR cavity to optimize the growth condition and measure the optical characteristics of MQWs. Initially, we started from s GaAs/AlAs four MQW structure, which is generally used in the microcavity structure using MBE growth. Figure 6 shows the PL spectra of only MQW structures at 5 K. The PL emission of the GaAs/AlAs MQW showed significant linewidth broadening. The measured linewidth is about 18.2 meV, which is larger than typical Rabi splitting values. Unlike MBE, the growth temperature in MOCVD is relatively high, which can cause severe intermixing between the adjacent layers when there is a large difference in composition. So, we reduced the Al composition in the barrier as $Al_{0.35}Ga_{0.65}As$. We have grown three sets of $GaAs/Al_{0.35}Ga_{0.65}As$ four MQWs (a total of 12 QWs). The linewidth of PL emission was decreased

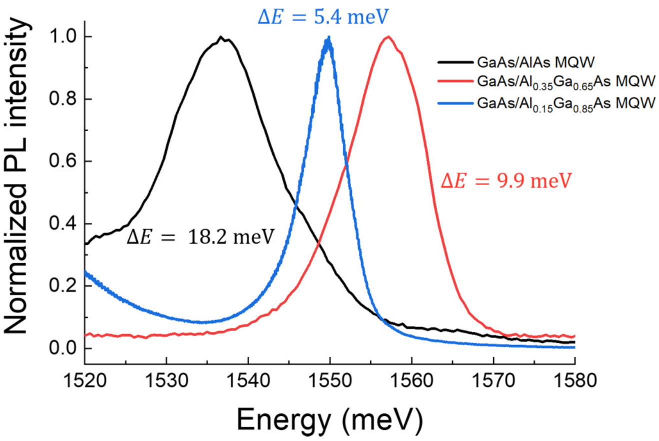

FIG. 6. PL spectrum of only MQW structure without DBR cavity at 5 K. There are three kinds of MQWs with different growth conditions. The linewidth of MQW emission is reduced from 18.2 to 5.4 meV after optimization.

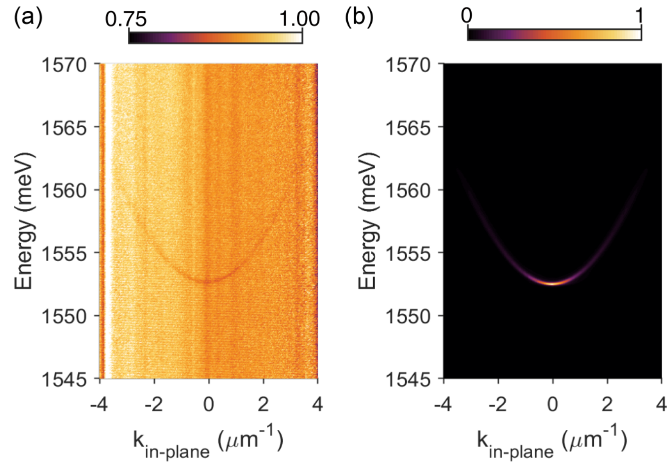

FIG. 7. Weak-coupling regime of microcavity with unoptimized MQWs. (a) Angle-resolved reflectance spectrum and (b) angle-resolved PL spectrum of the microcavity at 5 K. The microcavity contains $GaAs/Al_{0.35}Ga_{0.65}As$ MQWs.

to 9.9 meV. Furthermore, we increased the thickness of the well and barrier from 3.0 to 4.0 nm in the barrier, and 8.5 to 10.0 nm in the well, reducing the linewidth broadening [40]. Moreover, we further decreased the Al composition of the barrier to $Al_{0.15}Ga_{0.85}As$. We also decreased the growth rate and introduced growth interruption between each well and barrier layers in 5 s. Stopping the supply of the sources within a few seconds can flatten and make high-quality layer structures when growing thin structures [41]. And we have grown four MQWs to reduce variation from vertical MQW sets. Then, the linewidth of PL emission was reduced to 5.4 meV. With this condition, we successfully realized Rabi splitting in a full microcavity structure, which is shown in Fig. 2.

However, we could not observe anticrossing behavior with the unoptimized MQWs. We have also grown the microcavity with $GaAs/Al_{0.35}Ga_{0.65}As$ MQWs, which has 9.9 meV of the linewidth of PL emission, shown as the red curve in Fig. 6. This linewidth is similar to the Rabi splitting value reported in GaAs microcavities. So, the angle-resolved reflectance and PL spectra show clear parabolic signals, shown in Fig. 7, indicating that the microcavity is in a *weak*-coupling regime. We speculate that the linewidth of the unoptimized MQW grown inside the microcavity may not be narrow enough to meet the strong-coupling condition.

Although we showed the $3\lambda/2$ cavity in Fig. 2, we also obtained the smaller Rabi splitting value in the $\lambda/2$ cavity. We have grown the microcavity that contains $\lambda/2$ optical cavity between two DBRs consisting of 32.5 and 40 pairs of $AlAs/Al_{0.2}Ga_{0.8}As$. The cavity contains four MQWs in the antinode of an electric field. MQWs consist of $GaAs/Al_{0.15}Ga_{0.85}As$. We observed Rabi splitting in the angle-resolved reflectance spectrum, shown in Fig. 8. The measured Rabi splitting value is 5.8 meV. The interaction strength between the QW and cavity modes is proportional to the square of the number of MQWs, $\Omega_R \sim \sqrt{N_{\mathrm{QW}}}$ [42]. So, we could confirm that experimentally the tendencies of Rabi splitting values from 4 MQWs to 12 MQWs as 5.8 to 10.1 meV ($10.1/5.8 \sim \sqrt{3}$).

V. CONCLUSIONS

We successfully realize the polariton condensation even in the MOCVD-grown GaAs-based microcavity. We optimized the MQW quality to satisfy strong-coupling conditions with the DBR-based cavity. We reduced the linewidth of MQW emissions from 18.2 to 5.4 meV by changing growth designs and conditions. And we integrated optimized MQWs with a DBR-based microcavity having a few thousand of Q factor. In our microcavity, the measured Rabi splitting value is 10.1 meV and the measured Q factor is $\sim 9 \times 10^3$. Furthermore, we etched the part of the top DBR for observing anticrossing behavior and the upper polariton branches. We observed nonequilibrium condensation of polaritons above the threshold pumping power in angle-resolved PL spectroscopy. We also observed the nonlinear increase in PL intensity, linewidth narrowing, and blueshift according to pumping power. MOCVD has not been significantly considered in

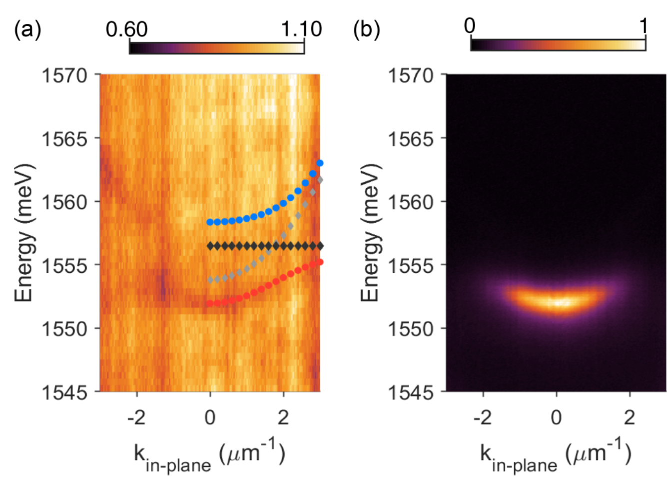

FIG. 8. Smaller Rabi splitting value in the $\lambda/2$ cavity. (a) Angle-resolved reflectance spectrum and (b) angle-resolved PL spectrum of the microcavity at 5 K. The microcavity contains four $GaAs/Al_{0.15}Ga_{0.85}As$ MQWs.

GaAs-based polariton condensation research because of the strong influence of MBE. From our results, we anticipate that MOCVD is able to grow the microcavities with high Q factors ($> 10^4$ order) through improvement in adding more DBR pairs or using longer cavities, such as a $5\lambda/2$ cavity. Considering the mass production ability and growth controllability of MOCVD, MOCVD can be effective for fabricating practical GaAs-based polariton devices with proper sample design and optimized growth conditions. Research on polariton devices has been continuously investigated for the past several decades. Through this result, we will be able to reevaluate the MOCVD growth method once again and open the way for the practical implementation of polariton devices.

ACKNOWLEDGMENTS

The authors thank Hwan-Seop Yeo, Hyun Gyu Song, Le Si Dang, and Maxime Richard for valuable comments and thank RayIR Co. Ltd. for discussing sample growth conditions. We acknowledge support from the National Research Foundation (NRF) of the Korea Government (Grants No. 2020M3E4A1080112 and No. 2022R1A2B5B03002560), the Samsung Science and Technology Foundation (Grant No. SSTF-BA1602-05), and the Institute of Information and Communications Technology Planning and Evaluation (IITP) grant funded by the Korea Government (MSIT) (Grant No. 2020-0-00841).

[1] J. Kasprzak, M. Richard, S. Kundermann, A. Baas, P. Jeambrun, J. M. Keeling, F. M. Marchetti, M. H. Szymanska, R. Andre, J. L. Staehli, V. Savona, P. B. Littlewood, B. Deveaud, and S. Dang le, Bose-Einstein condensation of exciton polaritons, Nature (London) **443**, 409 (2006).

[2] A. Amo, D. Sanvitto, F. P. Laussy, D. Ballarini, E. del Valle, M. D. Martin, A. Lemaitre, J. Bloch, D. N. Krizhanovskii, M. S. Skolnick, C. Tejedor, and L. Vina, Collective fluid dynamics of a polariton condensate in a semiconductor microcavity, Nature (London) **457**, 291 (2009).

[3] K. G. Lagoudakis, M. Wouters, M. Richard, A. Baas, I. Carusotto, R. André, L. S. Dang, and B. Deveaud-Plédran, Quantized vortices in an exciton–polariton condensate, Nat. Phys. **4**, 706 (2008).

[4] A. Amo, S. Pigeon, D. Sanvitto, V. Sala, R. Hivet, I. Carusotto, F. Pisanello, G. Leménager, R. Houdré, and E. Giacobino, Polariton superfluids reveal quantum hydrodynamic solitons, Science **332**, 1167 (2011).

[5] T. Jacqmin, I. Carusotto, I. Sagnes, M. Abbarchi, D. D. Solnyshkov, G. Malpuech, E. Galopin, A. Lemaître J. Bloch, and A. Amo, Direct observation of Dirac cones and a flatband in a honeycomb lattice for polaritons, Phys. Rev. Lett. **112**, 116402 (2014).

[6] H. Deng, G. Weihs, D. Snoke, J. Bloch, and Y. Yamamoto, Polariton lasing vs. photon lasing in a semiconductor microcavity, Proc. Natl. Acad. Sci. USA **100**, 15318 (2003).

[7] C. Schneider, A. Rahimi-Iman, N. Y. Kim, J. Fischer, I. G. Savenko, M. Amthor, M. Lermer, A. Wolf, L. Worschech, and V. D. Kulakovskii, An electrically pumped polariton laser, Nature (London) **497**, 348 (2013).

[8] S. Tsintzos, N. Pelekanos, G. Konstantinidis, Z. Hatzopoulos, and P. Savvidis, A GaAs polariton light-emitting diode operating near room temperature, Nature (London) **453**, 372 (2008).

[9] T. Gao, P. S. Eldridge, T. C. H. Liew, S. I. Tsintzos, G. Stavrinidis, G. Deligeorgis, Z. Hatzopoulos, and P. G. Savvidis, Polariton condensate transistor switch, Phys. Rev. B **85**, 235102 (2012).

[10] S. Klembt, T. Harder, O. Egorov, K. Winkler, R. Ge, M. Bandres, M. Emmerling, L. Worschech, T. Liew, and M. Segev, Exciton-polariton topological insulator, Nature (London) **562**, 552 (2018).

[11] S. Ghosh and T. C. H. Liew, Quantum computing with exciton-polariton condensates, npj Quantum Inf. **6**, 16 (2020).

[12] S. Christopoulos, G. B. H. Von Högersthal, A. Grundy, P. Lagoudakis, A. Kavokin, J. Baumberg, G. Christmann, R. Butté, E. Feltin, and J.-F. Carlin, Room-Temperature Polariton Lasing in Semiconductor Microcavities, Phys. Rev. Lett. **98**, 126405 (2007).

[13] S. Kéna-Cohen and S. Forrest, Room-temperature polariton lasing in an organic single-crystal microcavity, Nat. Photonics **4**, 371 (2010).

[14] R. Su, S. Ghosh, J. Wang, S. Liu, C. Diederichs, T. C. Liew, and Q. Xiong, Observation of exciton polariton condensation in a perovskite lattice at room temperature, Nat. Phys. **16**, 301 (2020).

[15] J. Zhao, R. Su, A. Fieramosca, W. Zhao, W. Du, X. Liu, C. Diederichs, D. Sanvitto, T. C. Liew, and Q. Xiong, Ultralow threshold polariton condensate in a monolayer semiconductor microcavity at room temperature, Nano Lett. **21**, 3331 (2021).

[16] R. Miller, D. Kleinman, W. Tsang, and A. Gossard, Observation of the excited level of excitons in GaAs quantum wells, Phys. Rev. B **24**, 1134 (1981).

[17] H. Suchomel, S. Kreutzer, M. Jörg, S. Brodbeck, M. Pieczarka, S. Betzold, C. Dietrich, G. Sęk, C. Schneider, and S. Höfling, Room temperature strong coupling in a semiconductor microcavity with embedded AlGaAs quantum wells designed for polariton lasing, Opt. Express **25**, 24816 (2017).

[18] C. Weisbuch, M. Nishioka, A. Ishikawa, and Y. Arakawa, Observation of the Coupled Exciton-Photon Mode Splitting in a Semiconductor Quantum Microcavity, Phys. Rev. Lett. **69**, 3314 (1992).

[19] H. Deng, G. Weihs, C. Santori, J. Bloch, and Y. Yamamoto, Condensation of semiconductor microcavity exciton polaritons, Science **298**, 199 (2002).

[20] R. Balili, V. Hartwell, D. Snoke, L. Pfeiffer, and K. West, Bose-Einstein condensation of microcavity polaritons in a trap, Science **316**, 1007 (2007).

[21] H. Cao, S. Pau, Y. Yamamoto, and G. Björk, Exciton-polariton ladder in a semiconductor microcavity, Phys. Rev. B **54**, 8083 (1996).

[22] G. Panzarini, L. C. Andreani, A. Armitage, D. Baxter, M. S. Skolnick, V. N. Astratov, J. S. Roberts, A. V. Kavokin, M. R. Vladimirova, and M. A. Kaliteevski, Exciton-light coupling in single and coupled semiconductor microcavities: Polariton dispersion and polarization splitting, Phys. Rev. B **59**, 5082 (1999).

[23] J. Dickerson, E. Mendez, A. Allerman, S. Manotas, F. Agulló-Rueda, and C. Pecharromán, Enhancement of Rabi splitting in a microcavity with an embedded superlattice, Phys. Rev. B **64**, 155302 (2001).

[24] A. V. Scherbakov, T. Berstermann, A. V. Akimov, D. R. Yakovlev, G. Beaudoin, D. Bajoni, I. Sagnes, J. Bloch, and M. Bayer, Ultrafast control of light emission from a quantum-well semiconductor microcavity using picosecond strain pulses, Phys. Rev. B **78**, 241302(R) (2008).

[25] Y. Sun, P. Wen, Y. Yoon, G. Liu, M. Steger, L. N. Pfeiffer, K. West, D. W. Snoke, and K. A. Nelson, Bose-Einstein Condensation of Long-Lifetime Polaritons in Thermal Equilibrium, Phys. Rev. Lett. **118**, 016602 (2017).

[26] P. Dapkus, A critical comparison of MOCVD and MBE for heterojunction devices, J. Cryst. Growth **68**, 345 (1984).

[27] F. Koyama, Recent advances of VCSEL photonics, J. Lightwave Technol. **24**, 4502 (2006).

[28] J. Pohl, G. D. Cole, U. Zeimer, M. Aspelmeyer, and M. Weyers, Reduction of absorption losses in MOVPE-grown AlGaAs Bragg mirrors, Opt. Lett. **43**, 3522 (2018).

[29] V. Dimastrodonato, L. O. Mereni, R. J. Young, and E. Pelucchi, AlGaAs/GaAs/AlGaAs quantum wells as a sensitive tool for the MOVPE reactor environment, J. Cryst. Growth **312**, 3057 (2010).

[30] A. V. Kavokin, J. J. Baumberg, G. Malpuech, and F. P. Laussy, *Microcavities* (Oxford University Press, New York, 2017), Vol. 21.

[31] G. C. DeSalvo, W. F. Tseng, and J. Comas, Etch rates and selectivities of citric acid/hydrogen peroxide on GaAs, $Al_{0.3}Ga_{0.7}As$, $In_{0.2}Ga_{0.8}As$, $In_{0.53}Ga_{0.47}As$, $In_{0.52}Al_{0.48}As$, and InP, J. Electrochem. Soc. **139**, 831 (1992).

[32] K. Bacher and J. Harris Jr., A wet etching technique for accurate etching of GaAs/AlAs distributed Bragg reflectors, J. Electrochem. Soc. **142**, 2386 (1995).

[33] J. Hopfield, Theory of the contribution of excitons to the complex dielectric constant of crystals, Phys. Rev. **112**, 1555 (1958).

[34] M. Wouters, I. Carusotto, and C. Ciuti, Spatial and spectral shape of inhomogeneous nonequilibrium exciton-polariton condensates, Phys. Rev. B **77**, 115340 (2008).

[35] H. G. Song, S. Choi, C. H. Park, S.-H. Gong, C. Lee, M. S. Kwon, D. G. Choi, K. Y. Woo, and Y.-H. Cho, Tailoring the potential landscape of room-temperature single-mode whispering gallery polariton condensate, Optica **6**, 1313 (2019).

[36] P. Tsotsis, P. S. Eldridge, T. Gao, S. I. Tsintzos, Z. Hatzopoulos, and P. G. Savvidis, Lasing threshold doubling at the crossover from strong to weak coupling regime in GaAs microcavity, New J. Phys. **14**, 023060 (2012).

[37] L. Tinkler, P. Walker, E. Clarke, D. Krizhanovskii, F. Bastiman, M. Durska, and M. Skolnick, Design and characterization of high optical quality InGaAs/GaAs/AlGaAs-based polariton microcavities, Appl. Phys. Lett. **106**, 021109 (2015).

[38] M. Steger, G. Liu, B. Nelsen, C. Gautham, D. W. Snoke, R. Balili, L. Pfeiffer, and K. West, Long-range ballistic motion and coherent flow of long-lifetime polaritons, Phys. Rev. B **88**, 235314 (2013).

[39] See Supplemental Material at http://link.aps.org/supplemental/10.1103/PhysRevResearch.4.033188 for more information about a tightly-focused pumping beam case and pumping power dependence of polariton condensates.

[40] S. A. Lourenço, M. A. T. da Silva, I. F. L. Dias, J. L. Duarte, E. Laureto, A. A. Quivy, and T. E. Lamas, Correlation between luminescence properties of $Al_xGa_{1-x}As/GaAs$ single quantum wells and barrier composition fluctuation, J. Appl. Phys. **101**, 113536 (2007).

[41] A. Jasik, A. Wnuk, A. Wójcik-Jedlińska, R. Jakieła, J. Muszalski, W. Strupiński, and M. Bugajski, The influence of the growth temperature and interruption time on the crystal quality of InGaAs/GaAs QW structures grown by MBE and MOCVD methods, J. Cryst. Growth **310**, 2785 (2008).

[42] R. Houdré, C. Weisbuch, R. Stanley, U. Oesterle, P. Pellandini, and M. Ilegems, Measurement of Cavity-Polariton Dispersion Curve from Angle-Resolved Photoluminescence Experiments, Phys. Rev. Lett. **73**, 2043 (1994).